Riboswitches

International Edition: DOI: 10.1002/anie.201507365
German Edition: DOI: 10.1002/ange.201507365

What a Difference an OH Makes: Conformational Dynamics as the Basis for the Ligand Specificity of the Neomycin-Sensing Riboswitch

*Elke Duchardt-Ferner[+], Sina R. Gottstein-Schmidtke[+], Julia E. Weigand, Oliver Ohlenschläger, Jan-Philip Wurm, Christian Hammann, Beatrix Suess, and Jens Wöhnert**

Dedicated to Matthias Görlach on the occasion of his 60th birthday

Abstract: *To ensure appropriate metabolic regulation, riboswitches must discriminate efficiently between their target ligands and chemically similar molecules that are also present in the cell. A remarkable example of efficient ligand discrimination is a synthetic neomycin-sensing riboswitch. Paromomycin, which differs from neomycin only by the substitution of a single amino group with a hydroxy group, also binds but does not flip the riboswitch. Interestingly, the solution structures of the two riboswitch–ligand complexes are virtually identical. In this work, we demonstrate that the local loss of key intermolecular interactions at the substitution site is translated through a defined network of intramolecular interactions into global changes in RNA conformational dynamics. The remarkable specificity of this riboswitch is thus based on structural dynamics rather than static structural differences. In this respect, the neomycin riboswitch is a model for many of its natural counterparts.*

Riboswitches are structured RNA elements that are mostly located in the 5′-untranslated regions of bacterial mRNAs. Upon binding to specific small-molecule ligands, they regulate gene expression at the level of transcription, translation, or RNA processing.[1]

Riboswitches constitute key nodes of metabolic regulation for controlling the cellular homoeostasis of coenzymes, signaling molecules, protein and nucleic acid building blocks, and ions. To ensure appropriate regulatory responses in a cellular environment, riboswitches must be able to discriminate efficiently between their cognate ligands and chemically similar molecules, even in situations where the latter are present in higher concentrations or when the structural differences between cognate and non-cognate ligands are very small.

In some cases, X-ray structures of riboswitch–ligand complexes directly reveal how the ligand binding pocket imposes strict steric restrictions to prevent the accommodation of ligand derivatives with even slight chemical/structural modifications.[2] However, in other cases, cognate and non-cognate ligands bind in a very similar manner and induce very similar tertiary structures in the bound RNA, despite differing strongly in their regulatory potency.[3]

In this study, we investigated the mechanism of ligand discrimination by the synthetic neomycin riboswitch with atomic resolution (Figure 1a).[4] In *S. cerevisiae*, this riboswitch represses translation initiation in response to the aminoglycosides neomycin (NEO) and ribostamycin (RIO).[4] However, it is regulatory inactive in the presence of paromomycin (PAR; Figure 1b), which differs from NEO only by the replacement of a single amino group at position 6′ with a hydroxy group (Figure 1c). Isothermal titration calorimetry shows that the riboswitch binds NEO with high affinity ($K_d = 10.0 \pm 2.0$ nM), whereas the affinity for PAR is significantly lower ($K_d = 5.1 \pm 0.3$ μM; Figure S1 in the Supporting Information). The replacement of one NH_3^+ group with an OH group thus results in an approximately 500-fold discrimination between these two ligands.

In order to understand the molecular basis for the remarkable ligand specificity of the neomycin riboswitch, we solved the structure of its complex with the regulatory-inactive ligand PAR by high-resolution solution NMR spectroscopy. We compared it to the structure of the regulatory-active RIO complex, which we solved previously and re-refined in the course of this work (see the Supporting Information).[5] Compared to NEO, RIO lacks ring IV (Figure 1c). However, the riboswitch forms structurally and dynamically very similar complexes with both regulatory-active ligands.[5b]

The high-resolution structure of the PAR–riboswitch complex (PDB ID 2MXS, Table S2 and Figure S2a in the Supporting Information), solved de novo to avoid potential model bias, superimposes very well with the structure of the

[*] Dr. E. Duchardt-Ferner,[+] Dr. S. R. Gottstein-Schmidtke,[+] Dr. J.-P. Wurm, Prof. Dr. J. Wöhnert
Institut für Molekulare Biowissenschaften and
Zentrum für Biomolekulare Magnetische Resonanz (BMRZ)
Goethe-Universität Frankfurt
Max-von-Laue Str. 9, 60438 Frankfurt/M (Deutschland)
E-mail: woehnert@bio.uni-frankfurt.de
Dr. J. E. Weigand, Prof. Dr. B. Suess
Fachbereich Biologie, Technische Universität Darmstadt
Schnittspahnstr. 10, 64287 Darmstadt (Deutschland)
Dr. O. Ohlenschläger
Biomolekulare NMR-Spektroskopie
Leibniz Institut für Altersforschung (Fritz-Lipmann-Institut)
Beutenbergstrasse 11, 07745 Jena (Deutschland)
Prof. Dr. C. Hammann
Ribogenetics Biochemistry Lab, Jacobs Universität Bremen
28759 Bremen (Deutschland)
[+] These authors contributed equally to this work.

Supporting information for this article (including experimental details) is available on the WWW under http://dx.doi.org/10.1002/anie.201507365.

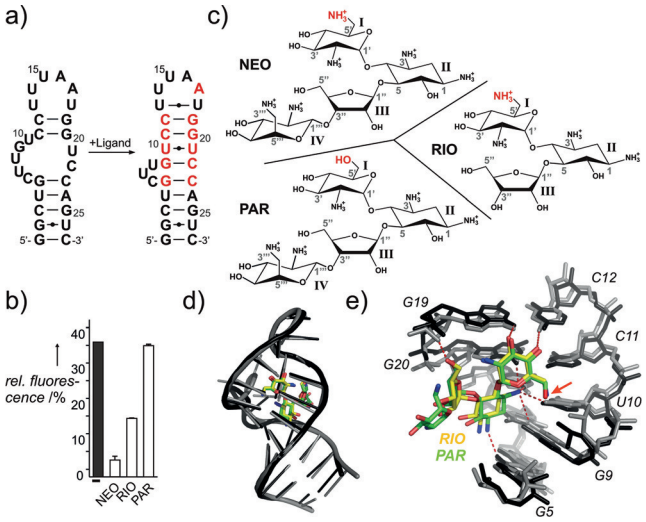

Figure 1. a) Secondary structure of the free and ligand-bound neomycin riboswitch. Residues involved in ligand binding are shown in red. b) Gene regulatory activity of the neomycin riboswitch in a GFP reporter gene assay in *S. cerevisiae* in the absence (black) or presence (white) of 100 μM NEO, RIO, or PAR. c) Structures of neomycin (NEO), paromomycin (PAR), and ribostamycin (RIO). The 6′ moieties are highlighted in red. d) Overlay of the 3D structures of the RIO–riboswitch (RNA in black; ligand carbons in yellow) and PAR–riboswitch (RNA in gray; ligand carbons in green) complexes. Ligand oxygen and nitrogen atoms are colored according to atom type. e) Binding pocket of the RIO–riboswitch (black) and PAR–riboswitch (gray) complexes. Hydrogen bonds are indicated by red lines; color scheme as in (d). The 6′ moiety is indicated by a red arrow.

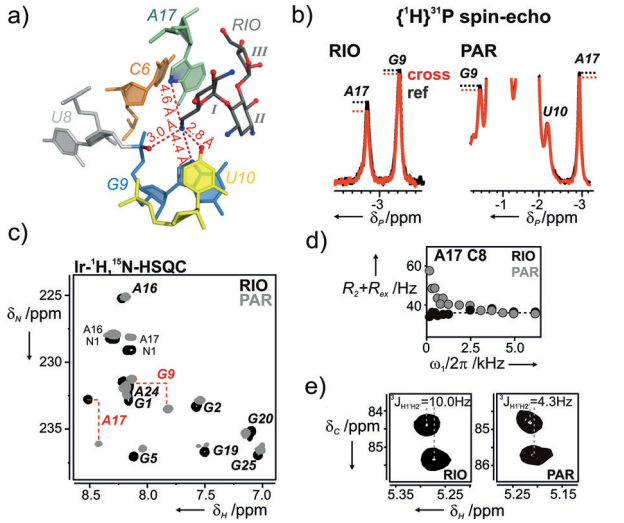

Figure 2. a) Spatial arrangement of RNA hydrogen bonding or electrostatic interactions in the vicinity of the 6′-NH_3^+ moiety in the RIO complex. Distances between the amino nitrogen and the acceptor groups are given. b) Section of quantitative ^{31}P-{^{1}H}-spin-echo spectra for the RIO (left) and PAR (right) complexes. Resonance assignments are given. The ^{1}H-decoupled reference experiments are shown in black, the coupling-attenuated cross experiments in red. c) Overlay of the N7 section of long-range ^{1}H-^{15}N HSQC spectra of the RIO (black) and PAR (gray) complexes. Purine H8/N7 correlations are assigned by residue name. Adenine H2/N1 correlations are labeled accordingly. For residues displaying strong chemical shift differences between the complexes, the resonances are labeled in red. d) "On-resonant spin-lock" dependent ^{13}C $R_{1\rho}$ relaxation dispersion profiles of C8 of A17 for the RIO (black) and PAR (gray) complexes. e) H1′/C2′ cross-peaks from HCCH-TOCSY-CCH-E.COSY spectra[11] of A17 of the RIO (left) and PAR (right) complexes. $^3J_{H,H}$ values extracted from the peak shifts in the proton dimension are indicated.

RIO complex (RMSD: ca. 0.5 Å; Figure 1d and Figure S2b), which is in agreement with very similar NOE cross-peak patterns and chemical shifts (Figures S3–S5). In both complexes, the two helical stems of the riboswitch RNA form one continuous A-form helix with stacking between the G5:C23 and G9:C22 base pairs, intersected by an internal loop consisting of C6 and the flexible nucleotides U7 and U8 (Figure S6). The apical loop (U14–U18) folds into a U-turn motif (U14–A16) entwined with a looped-out base motif (A16–U18), with A17 forming a flap on top of the ligand. The two ligands bind in a similar manner (Figure 1e Figure S5). In particular, the 6′ moiety of the ligand is located at a very similar position, close to the hinge region between the lower and the upper helical stems (Figure 1e), in both complexes. In the regulatory-active RIO complex, the positively charged[6] 6′-NH_3^+ group of RIO forms intermolecular hydrogen bonds with the 4-CO group of U10 and the negatively charged backbone phosphate group of G9 (Figure 2a,b), as well as intermolecular electrostatic interactions with the N7 moieties of G9 and A17. This is illustrated by the downfield shift of the signal for the 4-CO of U10[7] (Figure S7a) and the upfield shifts of the N7 resonances[8] of both G9 and A17 (Figure 2c).

For the regulatory-inactive PAR complex, quantitative 1D ^{31}P-{^{1}H}-spin-echo experiments[10] reveal a through-hydrogen-bond scalar $^{h2}J_{H,P}$ coupling for the G9 phosphate group (Figure 2b), which is in agreement with a hydrogen bond to the PAR 6′-OH group. The resonances for the 4-CO group of U10 and the N7 moieties of G9 and A17 are shifted to characteristic non-hydrogen-bonding positions (Figure 2c and Figure S7a). Thus, in contrast to the 6′-NH_3^+ group of RIO, the 6′-OH group of PAR contributes only one intermolecular interaction. The absence of an interaction between the ligand and N7 of A17 in the PAR complex has additional consequences. The nucleobase of A17, which is rigid on all time scales in the RIO complex (Figure 2d and Figure S6), displays motions on a μs time scale in the PAR complex (Figure 2d). The increased flexibility of the A17 nucleobase in the PAR complex is mirrored by an increased flexibility of the sugar moiety of A17 (Figure 2e and Figure S7b). Furthermore, the nucleobase of C6 from the internal loop is stably stacked on the A17 nucleobase in the RIO but not in the PAR complex (Figure S7c).

Surprisingly, the local loss of intermolecular interactions involving the 6′ group of the ligand does not only lead to local differences in RNA dynamics between the active and inactive complex. Apparent imino proton solvent exchange rates (Figure 3a, Figure S8 and Table S4) show that apart from the U10:U21 base pair in the binding site, remote parts of the RNA are also destabilized in the PAR complex compared to the RIO complex. At 30 °C, the imino protons of the U13:U18 base pair and U14 in the apical loop, which is connected to the ligand binding site through A17, show significantly higher exchange rates in the PAR complex. Correspondingly, when

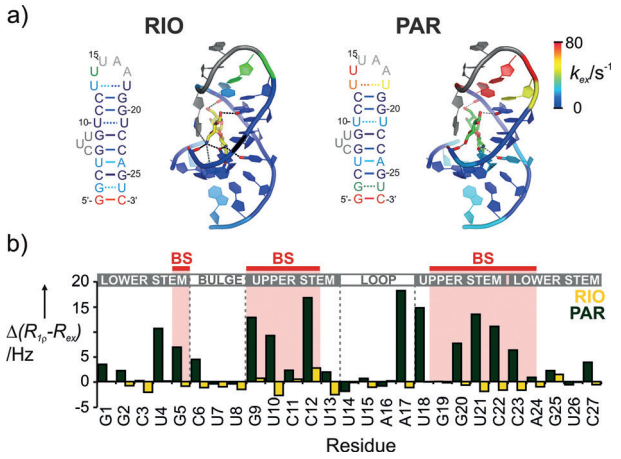

Figure 3. a) Imino proton solvent exchange rates for the RIO (left) and PAR (right) complexes at 30 °C. The exchange rates are color coded as indicated by the bar on the right side and plotted by base pair onto the 2D structure and residues 3–25 of the 3D structure. For the RIO and the PAR complexes, the ligands are shown in yellow and green, respectively. Intermolecular hydrogen bonding or electrostatic interactions are indicated by dashed lines. b) Differences between ^{13}C $R_{1\rho}$-values[9] measured at 25 Hz and at 1000 Hz effective spin-lock field strength of purine C8 and pyrimidine C6 spins in the RIO (yellow) and PAR (green) complexes. The structural elements of the RNA in the complex are indicated on top of the graph; binding-site residues are highlighted by red bars labeled BS.

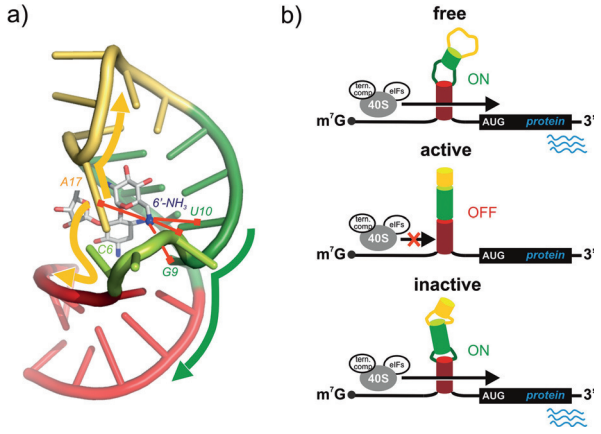

Figure 4. a) Stability network within the neomycin riboswitch that determines ligand activity. Direct interactions of the 6′-NH_3^+ group are shown in red, propagation of stabilization is shown as arrows. b) Model illustrating the conformational effects of the binding of regulatory-active (middle) and -inactive (bottom) ligands compared to the free riboswitch (top) and the consequences for riboswitch-mediated regulation of translation initiation by the 40S ribosomal subunit.

the interaction between the ligand 6′ group and N7 of A17 in the RIO complex is prevented by an A17C mutation, this also leads to destabilization of the entire apical loop and a significant subsequent reduction in regulatory activity (Figure S9).

Moreover, ^{13}C $R_{1\rho}$ relaxation rates for the PAR complex show a notable spin-lock field-strength dependence, not only for residues in the ligand binding site but also for U4 and G5 in the lower stem and U18 in the apical loop, thus suggesting the presence of μs to ms conformational exchange processes (Figure 3b, green). In contrast, for all residues of the RIO complex, no dependence of the $R_{1\rho}$ relaxation rates on the spin-lock field strength[9] is found, which is in line with a uniformly rigid structure (Figure 3b, yellow). Notably, the observed conformational exchange processes represent the dynamics of the bound state and are not due to ligand dissociation, since the corresponding k_{ex} rate constants obtained for selected residues (Figure S10) are much larger than any expected exchange contributions owing to ligand dissociation kinetics (see the Supporting Information). The latter process should also affect all residues in the binding pocket and the apical loop uniformly.

In summary, we conclude that the ligand specificity of the synthetic neomycin riboswitch is encoded at the level of structural dynamics. While an inactive ligand can induce the same average structure of the riboswitch, the absence of specific intermolecular interactions leads to local destabilization within the ligand binding site, which is then propagated into different structural elements of the riboswitch (Figure 4a).

The ability of an active ligand to stably connect all structural elements of the riboswitch immediately suggests a mechanism for its gene regulatory activity in vivo (Figure 4b): The free neomycin riboswitch—the regulatory ON state—adopts a weak hairpin structure consisting of two helical stems separated by an internal bulge (see Figure 1a). This structure can be easily dissolved by the scanning small ribosomal subunit (Figure 4b, top).[12] Binding of active as well as inactive ligands induces an elongation of the upper stem and coaxial stacking of the two stems. In complex with an active ligand, the neomycin riboswitch forms a continuously stabilized OFF-state structure, which offers steric resistance to the scanning small ribosomal subunit (Figure 4b, middle). In contrast, binding of an inactive ligand fails to stably connect the different structural elements of the neomycin riboswitch, thus resulting in a destabilized OFF-state complex, which can still be dissolved (Figure 4b, bottom). In addition, the faster k_{off} (Figure S11) for the inactive ligand reduces the lifetime of the ligand-bound state and increases the chance of the ribosome encountering a ligand-free riboswitch.

The small synthetic neomycin riboswitch shows a remarkable ability to discriminate between ligands differing only in a single functional group, which is comparable to the discriminatory power of structurally more complex natural riboswitches. Given that ligand-mediated coupling of separate structural domains appears to be a common feature for the interaction of riboswitches with their cognate ligands,[13] similar dynamics-based discrimination mechanisms may well be responsible for the ability to discriminate between the cognate ligands and closely related compounds in many other riboswitches.

Acknowledgements

We are grateful to Daniel Gottstein for support with structure calculations and to Harald Schwalbe for helpful discussions. This work was supported by the Aventis Foundation, the

Center for Biomolecular Magnetic Resonance (BMRZ) at the Goethe-University Frankfurt, grants from the Deutsche Forschungsgemeinschaft (WO901/2-1 to J.W., SU402/4-1 to B.S., and the Collaborative Research Center (SFB) 902 "Molecular principles of RNA based regulation"). The Fritz-Lipmann-Institute is financially supported by the Federal Government of Germany and the State of Thuringia.

Keywords: aminoglycoside · ligand specificity · riboswitches · RNA structures · structural biology

How to cite: *Angew. Chem. Int. Ed.* **2016**, *55*, 1527 – 1530
Angew. Chem. **2016**, *128*, 1551 – 1554

[1] a) R. R. Breaker, *Mol. Cell* **2011**, *43*, 867 – 879; b) K. E. Deigan, A. R. Ferre-D′Amare, *Acc. Chem. Res.* **2011**, *44*, 1329 – 1338.
[2] A. Serganov, D. J. Patel, *Annu. Rev. Biophys.* **2012**, *41*, 343 – 370.
[3] a) R. K. Montange, R. T. Batey, *Nature* **2006**, *441*, 1172 – 1175; b) R. K. Montange, E. Mondragon, D. van Tyne, A. D. Garst, P. Ceres, R. T. Batey, *J. Mol. Biol.* **2010**, *396*, 761 – 772; c) O. Pikovskaya, A. Polonskaia, D. J. Patel, A. Serganov, *Nat. Chem. Biol.* **2011**, *7*, 748 – 755; d) C. Lu, A. M. Smith, R. T. Fuchs, F. Ding, K. Rajashankar, T. M. Henkin, A. Ke, *Nat. Struct. Mol. Biol.* **2008**, *15*, 1076 – 1083.
[4] J. E. Weigand, M. Sanchez, E. B. Gunnesch, S. Zeiher, R. Schroeder, B. Suess, *RNA* **2008**, *14*, 89 – 97.
[5] a) S. R. Schmidtke, E. Duchardt-Ferner, J. E. Weigand, B. Suess, J. Wöhnert, *Biomol. NMR Assignments* **2010**, *4*, 115 – 118; b) E. Duchardt-Ferner, J. E. Weigand, O. Ohlenschläger, S. R. Schmidtke, B. Suess, J. Wöhnert, *Angew. Chem. Int. Ed.* **2010**, *49*, 6216 – 6219; *Angew. Chem.* **2010**, *122*, 6352 – 6355.
[6] F. Freire, I. Cuesta, F. Corzana, J. Revuelta, C. Gonzalez, M. Hricovini, A. Bastida, J. Jimenez-Barbero, J. L. Asensio, *Chem. Commun.* **2007**, 174 – 176.
[7] a) O. Ohlenschläger, J. Wöhnert, E. Bucci, S. Seitz, S. Häfner, R. Ramachandran, R. Zell, M. Görlach, *Structure* **2004**, *12*, 237 – 248; b) C. A. Theimer, L. D. Finger, L. Trantirek, J. Feigon, *Proc. Natl. Acad. Sci. USA* **2003**, *100*, 449 – 454.
[8] T. Dieckmann, E. Suzuki, G. K. Nakamura, J. Feigon, *RNA* **1996**, *2*, 628 – 640.
[9] A. L. Hansen, E. N. Nikolova, A. Casiano-Negroni, H. M. Al-Hashimi, *J. Am. Chem. Soc.* **2009**, *131*, 3818 – 3819.
[10] E. Duchardt-Ferner, J. Ferner, J. Wöhnert, *Angew. Chem. Int. Ed.* **2011**, *50*, 7927 – 7930; *Angew. Chem.* **2011**, *123*, 8073 – 8076.
[11] H. Schwalbe, J. P. Marino, S. J. Glaser, C. Griesinger, *J. Am. Chem. Soc.* **1995**, *117*, 7251 – 7252.
[12] M. Kozak, *Proc. Natl. Acad. Sci. USA* **1986**, *83*, 2850 – 2854.
[13] a) A. D. Garst, A. L. Edwards, R. T. Batey, *Cold Spring Harbor Perspect. Biol.* **2011**, *3*, a003533; b) A. Peselis, A. Serganov, *Biochim. Biophys. Acta Gene Regul. Mech.* **2014**, *1839*, 908 – 918.

Received: August 7, 2015
Published online: December 11, 2015

